Air Carbonisation of AC Electrochemical Copper and Aluminium Oxidation Products

N.V. Usoltseva, V.V. Korobochkin, M.A. Balmashnov
National Research Tomsk Polytechnic University, Tomsk, 634050, Russia

Abstract

The method for both simultaneous and separate electrochemical copper and aluminium oxidation using industrial frequency alternation current was developed. X-ray diffraction, IR spectroscopy and thermal analysis were used to determine the phase product composition. The electrochemical copper and aluminium oxidation results in the formation of cupreous oxide and aluminium oxyhydroxide, respectively. Air ageing of electrolysis products leads to dissolved carbon dioxide adsorption on their surfaces. Copper-aluminium carbonate hydroxide hydrate (Cu−Al/LDH) is the only copper-containing compound that is formed at the carbonization of simultaneous metal oxidation product. During heat treatment boehmite is continuously dehydrated by gamma-alumina at the temperature up to 500 °C. Heat treatment of copper oxidation product brings to the cupreous oxide oxidation by cupric oxide at 170−260 °C and malachite decomposition at 285−340 °C. It is required 150 °C to decompose Cu−Al/LDH completely.

Key words:

Alternating current electrolysis, copper oxides, aluminium oxides, layered double hydroxides, phase composition

1. Introduction

Layered double hydroxides are a family of materials that consist of positively charged mixed-metal hydroxide sheets. Positive charge is neutralized by negatively-charged anions which occupy the interlayer space together with water molecules that participate in hydrogen bonding of hydroxide layers. LDHs are represented by the general formula $\left[M^{II}_{1-x}M^{III}_{x}\ OH\ _2\right]^{x+}\left[A^{n-}_{x/n}\cdot yH_2O\right]^{x-}$, where M^{II} and M^{III} are divalent and trivalent metal cation respectively, A^{n-} is interlayer anions.

Layered double hydroxides are of current interest in different ways.

Both dried and thermally decomposed LDHs are widely used as catalysts for a variety of organic transformations [1−4]. LDHs are also utilized as adsorbents, ion exchangers, flame retardants, corrosion inhibitors [5−6]. There are some fields of LDH biological applications [7].

LDHs thermal decomposition results in the formation of highly active homogeneous mixed oxides with the great specific surface area, dispersion and sintering stability [6, 8−10].

Nowadays the attention is being paid to the systems with alumina as an effective catalyst support. Copper-containing oxide systems are active in hydrocarbon processing, gas purification from carbon and nitrogen oxides, wastewater purification from organic pollutants [11−14].

Among existence methods for metal oxide system production the non-equilibrium synthesis draws the scientist attention [15, 16]; one of them is the alternating current electrolysis [17].

The method for copper-aluminium oxide system production by simultaneous electrochemical copper and aluminium oxidation using industrial frequency alternation current was developed [18]. On air ageing under electrolyte solution, formed nano-sized copper-aluminium oxide system adsorbs the dissolved carbon dioxide and carbonization by copper-aluminium layered double hydroxides (Cu−Al/LDH) formation occurs [19].

To gain insight into structural properties of air carbonization products the X-ray diffraction, IR spectroscopy and thermal analysis have been performed.

2. Materials and Methods

Electrochemical metal oxidation by industrial frequency alternating current has been realized according to the method described in [18].

The synthetic procedure was as follows: electrochemical metal oxidation was carried out in sodium chloride solution with concentration of 3 wt % at the temperature of 90 °C and current density of 1 A cm^{-2}. At simultaneous electrochemical copper and aluminium oxidation the copper and aluminium plates were used as electrodes. At separate electrochemical copper or aluminium oxidation both electrodes were made of copper or aluminium, respectively.

Electrolysis products were washed with distilled water and air-dried at the temperature of 110 °C for 3 hours. The oven was naturally cooled to room temperature when the drying time was finished. Depending on sample phase composition, light blue, green or light blue with green colored tint solids were obtained.

Some electrolysis products were quickly deionized and dried at the residual pressure of 3−5 kPa to save the phase composition by preventing air phase transformation. Yellow solids were obtained in this case.

X-ray diffraction measurements (XRD) were performed on DRON-3M diffractometer operating at 25 mA and 35 kV, using CuK_α radiation (λ=1.5418 Å). Data were collected from 10 to 70° at a continuous scan rate of 4θ min^{-1}. PDF 2 database was used to identify the phase composition.

The FT-IR spectra were recorded on Nicolet 5700 equipped with a diffuse reflectance cell in the range of 4000−400 cm^{-1} at resolution of 4 cm^{-1}.

Thermogravimetric analysis (TGA) and differential scanning calorimetry (DSC) were carried out on thermal analyzer SDT Q600 in air at a heating rate of 10°C min^{-1} in the temperature range from ambient to 1000 °C except for the electrolysis products dried at the small residual pressure. These samples were heated up to 600−700 °C to prevent equipment from failure because of the sodium chloride residue melting.

3. Results and discussion

Fig. 1 shows the powder X-ray diffraction pattern of simultaneous electrochemical copper and aluminium oxidation product after quick washing from electrolyte ions and drying at the residual pressure of 3−5 kPa. Derived product consists of cupreous oxide Cu_2O (5-0667) and aluminium oxyhydroxide (boehmite, AlOOH, 17-0940).

Despite dominance of boehmite in the sample, XRD peaks of cupreous oxide are more intensive because of chemical properties of both cupreous oxide and boehmite. Sharp peaks of cupreous oxide grow from the high crystallinity of this compound whereas broad and diffuse peaks of boehmite point out the amorphism of its structure.

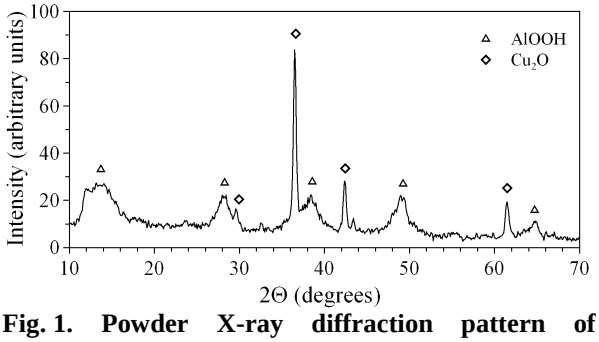

Fig. 1. Powder X-ray diffraction pattern of simultaneous electrochemical copper and aluminium oxidation product dried at the residual pressure of 3−5 kPa

Obtained cupreous oxide is yellow. Yellow color unlike red one is typical of cupreous oxide nanocrystals. The change of the color is going from the shift of the fundamental absorption edge towards the higher energies (blue shift). It is due to the band gap widening as a result of the quantum confinement effect [20, 21]. Separate copper oxidation also results to yellow cupreous oxide formation (fig. 2).

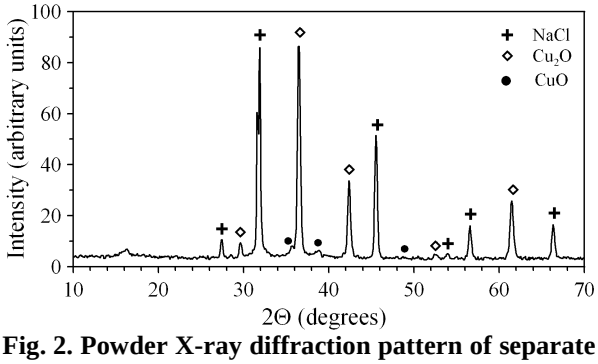

Fig. 2. Powder X-ray diffraction pattern of separate electrochemical copper oxidation product dried at the residual pressure of 3−5 kPa

In the opened air the dried cupreous oxide oxidizes to cupric oxide during 90 days [22]. Thermogravimetric analysis (TGA) and differential scanning calorimetry (DSC) show the cupreous oxide oxidizing to cupric oxide in the temperature range of 250−330 °C (fig. 3). Cupreous oxide formed by separate copper oxidation oxidizes at the lower

temperature of 220−290 °C (fig. 4). Increased cupreous oxide stability in product of simultaneous metal oxidation grows from Cu_2O interaction with boehmite. Thus, higher energy consumption is required to oxidize the cupreous oxide.

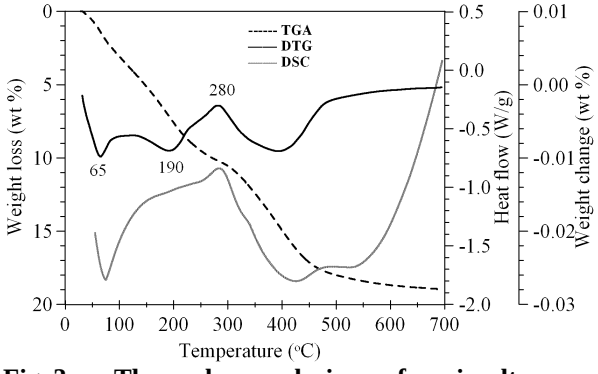

Fig. 3. Thermal analysis of simultaneous electrochemical copper and aluminium oxidation product dried at the residual pressure of 3−5 kPa

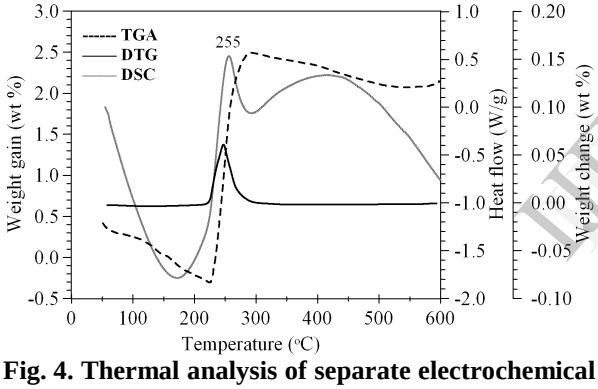

Fig. 4. Thermal analysis of separate electrochemical copper oxidation product dried at the residual pressure of 3−5 kPa

It is not typical of boehmite to lose the weight significantly in the temperature range of 130−230 °C. As it is shown below, small weight loss of air-dried product of separate aluminium oxidation is accompanied by great endothermic peak. Hence, significant weight loss of simultaneous metal oxidation product and small endothermic its peak results from the small power-consuming process. It may be the process of adsorbed carbon dioxide emission.

Fig. 5 shows powder X-ray diffraction patterns of air-dried products of both simultaneous and separate electrochemical oxidation of copper and aluminium. Experimental conditions and phase composition of the products are represented in the table.

Air-dried product of the separate electrochemical copper oxidation consists of cupric oxide CuO (5-0661), cupreous oxide Cu_2O (5-0667) and copper carbonate hydroxide (malachite) $Cu_2(OH)_2CO_3$ (41-1390) (fig. 5, V).

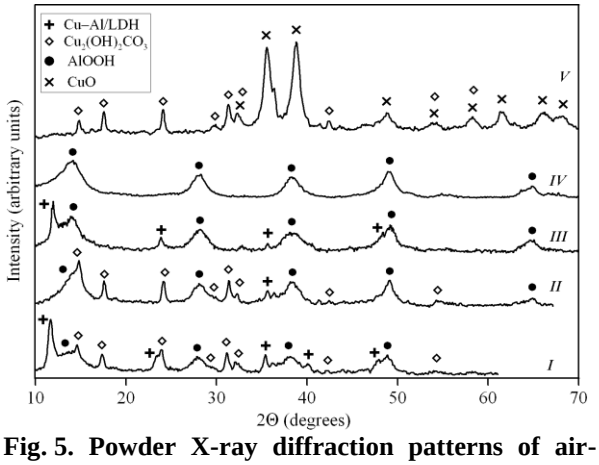

Fig. 5. Powder X-ray diffraction patterns of air-dried products of simultaneous electrochemical copper and aluminium oxidation

Table Experimental conditions and phase composition of air-dried products of electrochemical copper and aluminium oxidation

Sam.	Elec-trodes	Phase composition		
		AlOOH	Cu−Al/LDH	$Cu_2(OH)_2CO_3$
I	Cu–Al	+	+	+
II	Cu–Al	+	–	+
III	Cu–Al	+	+	–
IV	Al–Al	+	–	–
V	Cu–Cu	–	–	+
Sample II is the sample I after heat treatment at the temperature of 150 °C				

Aluminium oxyhydroxide (boehmite) AlOOH (17-0940) is the only indexed phase on the XRD pattern of separate electrochemical aluminium oxidation product (fig. 5, IV).

According to X-ray phase analysis the carbonization of electrolysis product with copper-aluminium carbonate hydroxide hydrate $Cu_{2,5}Al_2C_{1,7}O_{8,9}\cdot 5,2H_2O$ (46-0099) formation occurs at air ageing under electrolyte solution (fig. 5, I−III). This compound belongs to the family of layered double hydroxides. Its structure is formed by mixed layers of copper and aluminium hydroxides and carbonate ions between them (Cu−Al/LDH) [9]. Under some conditions copper carbonate hydroxide $Cu_2(OH)_2CO_3$ (41-1390) is formed in addition to Cu−Al/LDH (fig. 5, I). Boehmite content exceeds its content required to copper-aluminium carbonate

hydroxide hydrate formation. Therefore, product of carbonization contains excess of boehmite.

After heat treatment at 150 °C no reflections of any copper-containing compounds are indexed on the XRD pattern. It is due to cupric oxide as a product of Cu−Al/LDH destruction is x-ray amorphous.

High affinity of carbonate ions to some oxyhydroxides results in these ions adsorption on oxyhydroxide surface. The most intensive carbonization occurs by solution carbonate ions, but the adsorption of air carbon dioxide is also take place [23]. The absent of aluminium carbonate and aluminium carbonate hydroxide is explained by their instability because they are completely hydrolyzed to sparingly soluble aluminium hydroxide. In this case air carbon dioxide is only adsorbed on the surface and cannot be indexed by X-ray phase analysis. In this case IR spectroscopy may be used to clarify the adsorption of carbon dioxide (fig. 6). Aluminium oxyhydroxide is characterized by cation consumption, sodium particularly. Both carbonate ions and cations adsorption results in formation of sodium aluminium carbonate hydroxide $NaAl(CO_3)(OH)_2$ (19-1175) [24, 25]. The sensitivity of X-ray phase analysis is not high enough to detect the small amount of this compound. Nevertheless, $NaAl(CO_3)(OH)_2$ formation is confirmed by infrared spectroscopy (fig. 6).

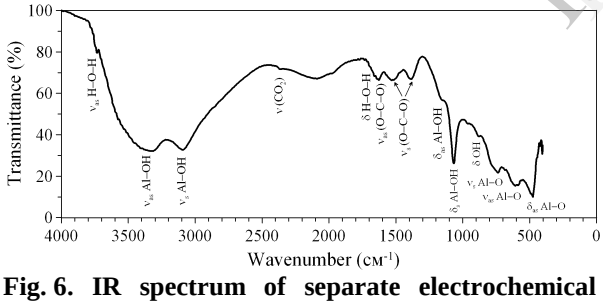

Fig. 6. IR spectrum of separate electrochemical aluminium oxidation product

Wide range of stretching OH vibrations (3800−2000 cm^{-1}) is due to the high sensitivity of electron cloud of OH bond to intermolecular interaction. The position of adsorption bands depends on strength of the hydrogen bond formed by OH groups [26]. On boehmite surface hydroxide ions are obtained and they are situated on ribs and connected with one aluminium cation. There are two kinds of hydroxide ions on faces, one of which is connected with two and another with three aluminium cations. As coordination of oxygen ion via aluminium is increased the frequency of stretching OH vibrations is decreased. Hence, hydroxyls connected with one aluminium cation are characterized by stretching vibration of 3660 cm^{-1}. It is not possible to identify this bend with our IR spectrum because of its low intensity. Bands with the maxima at 3300 и 3100 cm^{-1} corresponds to stretching vibration of hydroxyls connected with two and three aluminium cations, respectively [27].

The strong band at 1150 cm^{-1} and the shoulder at 1065 cm^{-1} are respectively assigned to asymmetric (δ_{as} Al–OH) and symmetric (δ_s Al–OH) bending vibrations of bulk O-H of boehmite, the weak band at 880 cm^{-1} is assigned to stretching vibrations of superficial O-H (δ OH). The bands 740, 620 и 480 cm^{-1} are respectively assigned to symmetric (ν_s Al–O) and asymmetric (ν_{as} Al–O) bending vibrations and stretching (δ_{as} Al–O) vibration of aluminium-oxigen bond [28].

According to [27], broad band in the range of 2300–1800 cm^{-1} is assigned to interlaminar hydrogen bonded OH vibrations of boehmite. Hydrogen bond causes reduction in OH vibration amplitude and decrease of absorption band intensity of related hydroxyls in comparison with free hydrohyls.

Absorption band in the range of 2385−2340 cm^{-1} is assigned to adsorbed carbon dioxide.

Coordinatively unsaturated cation and anion centres of boehmite absorb respectively air water molecules and carbon dioxide in the undissociated form. The set of absorption bands in the range of 3760–3720 cm^{-1} is assigned to asymmetric stretching vibrations of water molecules ν_{as} H−O−H, whereas absorption band in the range of 1725–1595 cm^{-1}corresponds to their bending vibrations δ H–O–H.

Broad absorption bands without clear maxima in the ranges of 1725–1595 cm^{-1}, 1590−1450 cm^{-1} and 1450−1300 cm^{-1} represent the overlay of some absorption bands. Interaction of air carbon dioxide with coordinatively unsaturated anion centres of boehmite results in monodentate carbonite formation and gives rise of absorption band (1650−1600 cm^{-1}) of asymmetric stretching vibrations of monodentate carbonite (ν_{as} O−C−O) against the background of absorption band of water molecule bending vibrations [29].

Absorption band in the ranges of 1450−1300 cm^{-1} represents the overlay of absorption band of symmetric stretching vibrations of monodentate carbonite (ν_s O−C−O) and asymmetric stretching vibrations of carbonate ions that belong to sodium aluminium carbonate hydroxide [24, 25]. Absorption band in the ranges of 1590−1450 cm^{-1} is assigned to combination of absorption band of stretching OH vibrations of sodium aluminium carbonate hydroxide and of

absorption band that arises from splitting of ν_s O−C−O due to interlayerspace disordering.

The IR-spectrum of electrochemical copper oxidation products was recorded to identify of the malachite absorption bands (fig. 7).

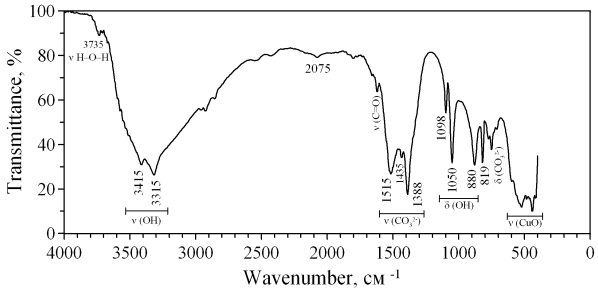

Fig. 7. IR spectrum of separate electrochemical copper oxidation product

Despite the fact that product of electrochemical copper oxidation is multicomponent (fig. 5, V), characteristic IR bands of malachite have not overlapped with ones of copper oxides. Hence, it is possible to identify required carbonate compound in the presence of copper oxides.

There are bands of stretching OH vibrations of malachite against the background of the bands of hydrogen bonded OH vibrations: bands in the ranges of 3440−3395 cm^{-1} with the maximum at 3415 cm^{-1} and bands in the ranges of 3350−3275 cm^{-1} with the maximum at 3315 cm^{-1}. Bands with the maxima at 1098, 1050 cm^{-1} are assigned to bending OH vibrations of malachite. Crystal structure of malachite consists of two types of disordered octahedrons. Hence, OH groups occupy two positions in this structure [30, 31]. Bands at the lower wavenumbers (3315 cm^{-1}, 1050 cm^{-1}) are assigned to OH groups connected by stronger hydrogen bond and absorption bands at the higher wave numbers (3415 cm^{-1}, 1098 cm^{-1}) are assigned to OH groups connected by weaker hydrogen bond. Likewise boehmite, absorption band with the maximum at 880 cm^{-1} (δ OH) is assigned to bending vibrations of surface OH groups that are not form malachite.

Absorption bands in the ranges of 3760–3720 cm^{-1} и 1725–1595 cm^{-1} are assigned to asymmetric stretching (ν_{as} H−O−H) and bending (δ H−O−H) vibrations of water molecules. δ H−O−H is overlapped by narrow band of C=O in the range of 1630−1610 cm^{-1}.

The sets of the bands 1515, 1435, 1388 cm^{-1}; 773, 750, 710 cm^{-1}; 820 cm^{-1} corresponds to asymmetric stretching vibrations (ν_3), in-plane (ν_4) and out-of-plane (ν_2) bending vibrations of carbonate-ions, respectively [31]. The splitting of carbonate absorption bands as that of OH absorption bands is due to malachite structure.

The set of absorption bands (598, 520, 483, 440 cm^{-1}) is assigned to stretching Cu−O vibrations.

As structure of malachite is not layered, absorption band with the maximum at 2075 cm^{-1} cannot be assigned to interlayer hydroxides. Thus, narrow absorption band in the IR spectrum of malachite in the range of 2230–1970 cm^{-1} is assigned to composite vibrations of water molecules because of changes of valence bond lengths and angels between them [27].

Malachite absorption bands in samples I−III are against the background of characteristic IR bands of boehmite (fig. 8). It arises from predominance of boehmite in these samples.

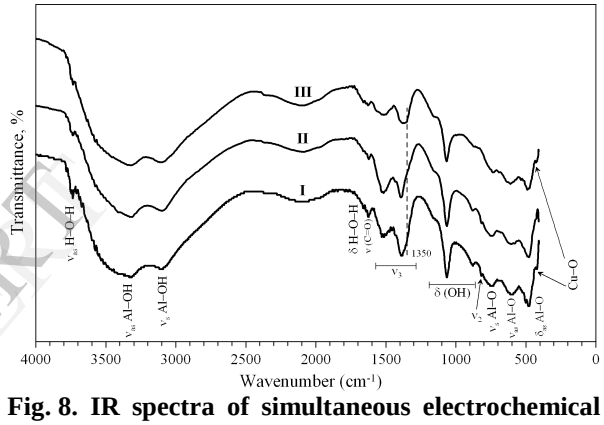

Fig. 8. IR spectra of simultaneous electrochemical copper and aluminium oxidation products

It was reliably stated by X-ray diffraction that malachite is the part of air-aged product of simultaneous electrochemical copper and aluminium oxidation (table, samples I and II). To detect absorption bands of malachite in sample I and II their IR spectra were compared with IR spectrum of sample V that preferably consists of absorption bends of malachite. Characteristic IR bands of malachite are 1630–1610 cm^{-1}, 1515, 1435, 1390 и 820 cm^{-1} [31].

Layered double hydroxide in samples I and III was identified by shoulder of absorption bend (1440−1300 cm^{-1}) at 1350 cm^{-1} that corresponds to asymmetric stretching vibration of interlaminar carbonate ν_{as} (CO_3^{2-}). Reduction of the symmetry in interlaminar space is the reason of absorption bend shift to longer wavelength (smaller wavenumber) relatively its position of free carbonate ions [9]. Also there is increased absorption of carbonate ions in the range of 3450−3300 cm^{-1} and absorption bend at 420 cm^{-1} due to vibration of metal-oxygen bond in the layer of LDH [32].

Thermal analysis was performed to estimate the thermal stability of compounds that form the product of electrolysis (fig. 9−11). The comparison of thermal analysis results of different composition samples contributed to identification of exo and endo effects.

According to thermal analysis (fig. 9) the removal of boehmite free moisture occurs at the temperature up to 110 °C. Endo effect and weight loss reach the maxima at the temperature 75−80 °C. As the temperature rises, both stepwise decomposition and continuous weight loss of boehmite occur up to 500 °C. Endo effects in the ranges of 135−300 °C, 300−500 °C corresponds to the loss of moisture that is generated as boehmite is decomposed to alumina.

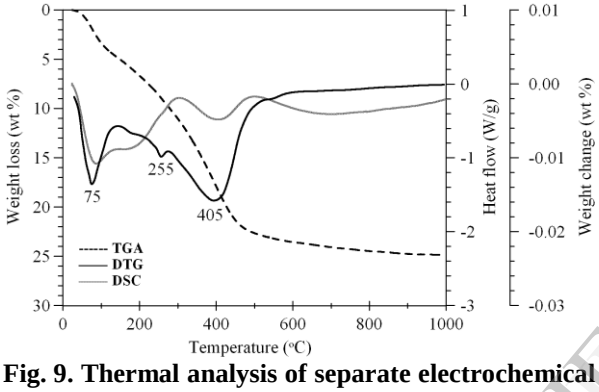

Fig. 9. Thermal analysis of separate electrochemical aluminium oxidation product

Defective structure of boehmite causes significant moisture adsorption on its highly-developed surface. While products of copper oxidation (copper oxides, copper carbonate hydroxide) do not have high specific surface area, it is not typical of them to adsorb a great amount of moisture. Thus, the differential thermogravimetric and differential scanning calorimetry curve donot have characteristic peak of weight loss and of endo effect, respectively (fig. 10).

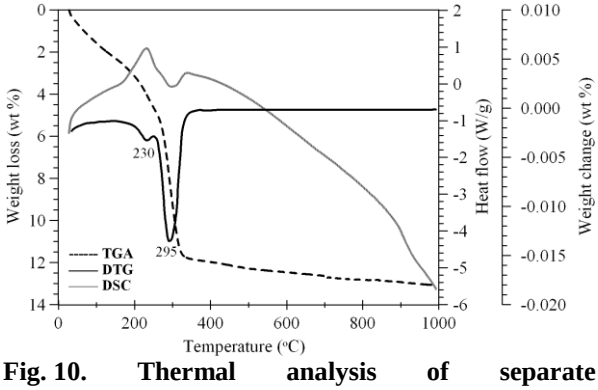

Fig. 10. Thermal analysis of separate electrochemical copper oxidation product

Broad exo effect within the entire temperature range corresponds to crystallization of nanocrystalline cupric oxide (fig. 10). There are some effects against it. The increase of the sample weight from cupreous oxide oxidation in the range of 170−260 °C is hidden by emission of adsorbed carbon dioxide whereas heat flow of oxidation process significantly exceeds to consumption of intrinsic system energy on carbon dioxide desorption. Endo effect and weight loss in the range of 285−340 °C corresponds to malachite decomposition.

Elimination of physically adsorbed water of boehmite from copper-containing sample I−III requires smaller energy consumption. As consequence, the maxima of the peaks are sifted to 65 °C (fig. 11).

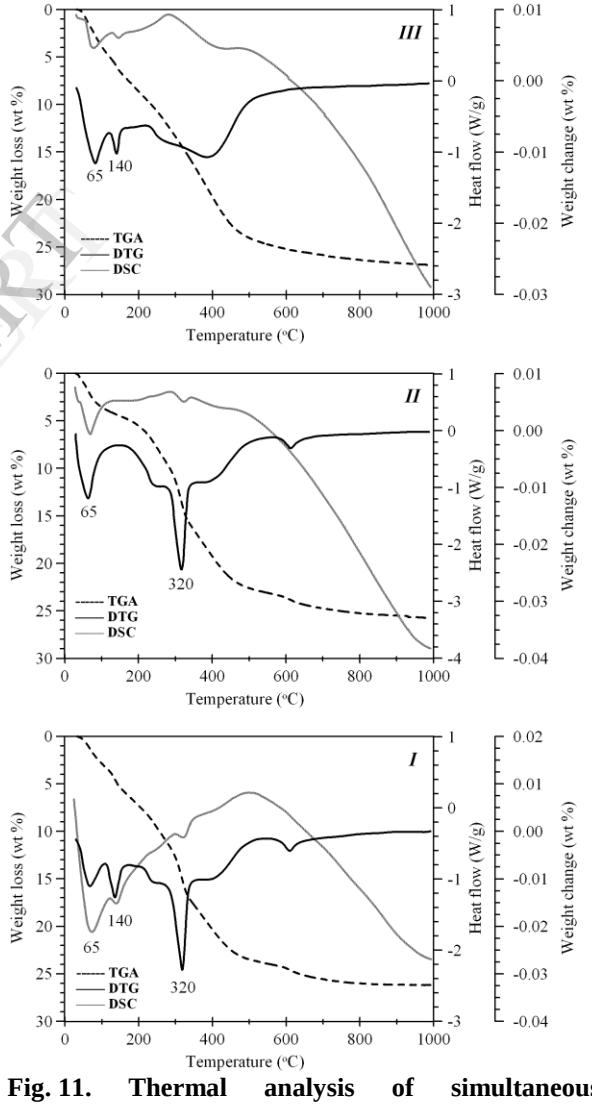

Fig. 11. Thermal analysis of simultaneous electrochemical copper and aluminium oxidation products

The influence of copper compounds on the temperature of physically adsorbed water elimination is confirmed by the thermal analysis of simultaneous electrochemical copper and aluminium oxidation products formed at the current density from 0.5 to 2.5 A/cm^2 [33]. Low oxidation rate of copper at 0.5 A/cm^2 results in absent of copper-species or such a low their content that they cannot be indexed by X-ray diffraction. The temperature of physically adsorbed water elimination from sample prepared at 0.5 A/cm^2 coincides with that from pure boehmite. At the higher current density the copper oxidation rate is high enough for the marked amount of copper species formation. The peaks of physically adsorbed water elimination on DTG/DSC curves of these samples are shifted to the lower temperature. The positions of own boehmite peaks on DSC/DTG curves correspond to that of pure boehmite (sample IV).

4. Conclusion

Products of non-equilibrium electrochemical copper and aluminium oxidation are spontaneously carbonized at the air ageing under electrolyte solution. Carbonization of separate copper oxidation product results in malachite formation. Carbon dioxide is preferably adsorbed on the product of separate aluminium oxidation, but some amount of sodium aluminium carbonate hydroxide $NaAl(CO_3)(OH)_2$ is formed. The main product of spontaneous carbonization of copper-aluminium oxide system formed by simultaneous copper and aluminium oxidation is the copper-aluminium carbonate hydroxide hydrate that belongs to the family of layered double hydroxides.

5. Acknowledgments

The authors thank Viktor Ignatov (PhD, Institute of High Technology Physics, National Research Tomsk Polytechnic University) for help in X-ray diffraction measurements, TPU Scientific and analyzing center for carrying out thermal analysis and IR spectroscopy of the samples (FTP GC №16.552.11.7063).

6. Literature

[1] Segal S.R., Carrado K.A., Marshall Ch.L., Anderson K.B. (2003) Catalytic decomposition of alcohols, including ethanol, for in situ H_2 generation in a fuel stream using a layered double hydroxide-derived catalyst, Appl. Cat. A Gen., 248(1-2), 33-45.

[2] Likhar P.R., Arundhathi R., Kantam M.L., Prathima P.S. (2009) Amination of alcohols catalyzed by copper-aluminium hydrotalcite: A green synthesis of amines. Eur. J. Org. Chem., 31, 5383-5389.

[3] Xu Zh.P, Zhang Ji., Adebajo M.O., Zhang H., Zhou Ch. (2011) Catalytic applications of layered double hydroxides and derivatives. Appl Clay Sci., 53(2), 139-150.

[4] Zhou Ch.-H., Beltramini Jo.N., Lin Ch.-X., Xu Zh.-P., Lu (Max) G.Q., Tanksale A. (2011) Selective oxidation of biorenewable glycerol with molecular oxygen over Cu-containing layered double hydroxide-based catalysts. Catal. Sci. Technol., 1, 111-122.

[5] Zhu H., Wang W., Liu T. (2011) Effects of copper-containing layered double hydroxide on thermal and smoke behavior of poly(vinyl chloride). J. Appl. Polym. Sci., 122(1), 273-281.

[6] Bergaya F., Theng B.K.G., Lagaly G. (2006) Developments in clay science. V. 1. Handbook of clay science. Amsterdam, Elsevier Science

[7] Choy Ji.-H., Choi S.-Ji., Oh Ja.-M., Park T. (2007) Clay minerals and layered double hydroxides for novel biological applications. Appl. Clay Sci., 36(1-3), 122-132.

[8] Duan X., Evans D.G. (ed) (2006) Structure and bonding. Vol. 119. Layered double hydroxides. Berlin, Heidelberg, Springer-Verlag Berlin Heidelberg

[9] Auerbach S.M., Carrado K.A., Dutta P.K. (ed) (2004) Handbook of layered materials. Marcel Dekker, New York

[10] Rives V. (2001) Layered double hydroxides: present and future. Nova Science Publisher, New York

[11] Bradu C., Frunza L., Mihalche N., Avramescu S.-M., Neață M., Udrea I. (2010) Removal of Reactive Black 5 azo dye from aqueous solutions by catalytic oxidation using CuO/Al_2O_3 and NiO/Al_2O_3. Appl. Catal. B Environ., 96(3-4), 548-556

[12] Massa P.A., Ayude M.A., Fenoglio R.J., Gonzalez J.F., Haure P.M. (2004) Catalyst systems for the oxidation of phenol in water. Lat. Am. Appl. Res., 34(3), 133-140.

[13] Segal S.R., Anderson K.B., Carrado K.A., Marshall Ch.L. (2012) Low temperature steam reforming of methanol over layered double hydroxide-derived catalysts. Appl. Catal. A Gen., 231(1-2), 215-226.

[14] Kovanda F., Jiratova K. (2011) Supported layered double hydroxide-related mixed oxides and their application in the total oxidation of volatile organic compounds. Appl. Clay Sci., 53(2), 305-316.

[15] Zyryanov V.V. (2008) Mechanochemical synthesis of complex oxides. Russ. Chem. Rev., 77(2), 107-137.

[16] Sytschev A.E., Merzhanov A.G. (2004) Self-propagating high-temperature synthesis of nanomaterials. Russ. Chem. Rev., 73(2), 157-170.
[17] Korobochkin V.V. (2004) Processes of nanodispersed oxide obtaining using alternating current electrochemical oxidation of metals: diss. … doctor of engineering science, Tomsk Polytechnic University, Russia
[18] Korobochkin V.V., Usoltseva N.V., Balmashnov M.A. (2012) Non-equilibrium electrochemical synthesis of copper-aluminium oxide system. Fundamental research 11(1), 143-147.
[19] Korobochkin V.V., Usoltseva N.V., Balmashnov M.A. (2012) Phase composition of nanosized products of non-equilibrium electrochemical oxidation of copper and aluminum. Bul. Tomsk polytech. university. Chem., 321(3), 59-63.
[20] Borgohain K., Murase N., Mahamuni Sh. (2002) Synthesis and properties of Cu_2O quantum particles. J. Appl. Phys., 92(3), 1292-1297.
[21] Kuo Ch.-H., Huang M.H. (2008) Facile synthesis of Cu_2O nanocrystals with systematic shape evolution from cubic to octahedral structures. J. Phys. Chem. C., 112(47), 18355-18360.
[22] Usoltseva N.V., Korobochkin V.V., Balmashnov M.A. (2013) Microstructure of material formed by non-equilibrium electrochemical oxidation of copper and aluminium. Fundamental research, 8(3), 750–755.
[23] Pechenuk S.I., Budnikov N.A. (2006) Carbonate ion adsorption by oxyhydroxides of iron (III) and aluminum. Bulletin of the South Ural state university 7, 233-238.
[24] Estep P.A., Karr C. (1968) The infrared spectrum of dawsonite. The American mineralogist, 53, 305-309.
[25] Su Ch., Suarez D.L. (1997) In situ infrared speciation of adsorbed carbonate on aluminum and iron oxides. Clays and Clay Minerals 45(6), 814-825.
[26] Plusnina I.I. (1976) Infrared spectra of minerals. Moscow state University, Moscow
[27] Chukin G.D. (1976) Structure of the surface of γ-alumina. J. Struct. Chem., 17(1), 99-104.
[28] Hou H, Xie Yi, Yang Q, Guo Q, Tan Ch (2005) Preparation and characterization of $\gamma-AlOOH$ nanotubes and nanorods. Nanotechnol., 16(6), 741-745.
[29] Morterra C., Emanuel C., Cerrato G., Magnacca G. (1992) Infrared study of some surface properties of boehmite ($\gamma-AlO_2H$). J. Chem. Soc., Faraday Trans., 88, 339-348.
[30] Ivanova V.P., Kasatov B.K., Krasavina T.N., Rozinova E.L. (1974) Thermal analysis of minerals and rocks. Nedra, Leningrad
[31] Schmidt M., Lutz H.D. (1993) Hydrogen bonding in basic copper salts: a spectroscopic study of malachite, $Cu_2(OH)_2CO_3$, and brochantite, $Cu_4(OH)_6SO_4$. Phys. Chem. Minerals, 20(1), 27-32.
[32] Trujillano R., Holgado M.J., Pigazo F., Rives V. (2006) Preparation, physicochemical characterisation and magnetic properties of Cu–Al layered double hydroxides with CO_3^{2-} and anionic surfactants with different alkyl chains in the interlayer. Physica B, 373(2), 267-273.
[33] Korobochkin V.V., Usoltseva N.V., Balmashnov M.A. (2013) Texture of carbonate precursors of copper-aluminum oxide system obtained from the products of non-equilibrium electrochemical oxidation of copper and aluminum. Bul. Tomsk polytech. university. Chem., 322(3), 100-104.
[34] Britto S.P., Kamath V. (2009) Thermal, solution and reductive decomposition of Cu–Al layered double hydroxides into oxide products. J. Solid State Chem., 182(5), 1193-1199.